npg

ORIGINAL ARTICLE

Phytoplankton distribution patterns in the northwestern Sargasso Sea revealed by small subunit rRNA genes from plastids

Alexander H Treusch[1,5], Elif Demir-Hilton[2], Kevin L Vergin[1], Alexandra Z Worden[2], Craig A Carlson[3], Michael G Donatz[4], Robert M Burton[4] and Stephen J Giovannoni[1]

[1]Department of Microbiology, Oregon State University, Corvallis, OR, USA; [2]Monterey Bay Aquarium Research Institute, Moss Landing, CA, USA; [3]Department of Ecology, Evolution and Marine Biology, University of California, Santa Barbara, CA, USA and [4]Department of Mathematics, Oregon State University, Corvallis, OR, USA

Phytoplankton species vary in their physiological properties, and are expected to respond differently to seasonal changes in water column conditions. To assess these varying distribution patterns, we used 412 samples collected monthly over 12 years (1991–2004) at the Bermuda Atlantic Time-Series Study site, located in the northwestern Sargasso Sea. We measured plastid 16S ribosomal RNA gene abundances with a terminal restriction fragment length polymorphism approach and identified distribution patterns for members of the Prymnesiophyceae, Pelago-phyceae, Chrysophyceae, Cryptophyceae, Bacillariophyceae and Prasinophyceae. The analysis revealed dynamic bloom patterns by these phytoplankton taxa that begin early in the year, when the mixed layer is deep. Previously, unreported open-ocean prasinophyte blooms dominated the plastid gene signal during convective mixing events. Quantitative PCR confirmed the blooms and transitions of Bathycoccus, Micromonas and Ostreococcus populations. In contrast, taxa belonging to the pelagophytes and chrysophytes, as well as cryptophytes, reached annual peaks during mixed layer shoaling, while Bacillariophyceae (diatoms) were observed only episodically in the 12-year record. Prymnesiophytes dominated the integrated plastid gene signal. They were abundant throughout the water column before mixing events, but persisted in the deep chlorophyll maximum during stratified conditions. Various models have been used to describe mechanisms that drive vernal phytoplankton blooms in temperate seas. The range of taxon-specific bloom patterns observed here indicates that different 'spring bloom' models can aptly describe the behavior of different phytoplankton taxa at a single geographical location. These findings provide insight into the subdivision of niche space by phytoplankton and may lead to improved predictions of phytoplankton responses to changes in ocean conditions.

Introduction

The composition of phytoplankton blooms, and the factors that control them, are both important aspects of global primary production. Several theories have been proposed to describe the physical–biological interactions controlling the timing of vernal (spring) blooms in seasonal seas for the phytoplankton community as a whole. One of these, Sverdrup's

Correspondence: SJ Giovannoni, Department of Microbiology, Oregon State University, Nash Hall, Corvallis, OR 97331, USA.
E-mail: steve.giovannoni@oregonstate.edu
[5]Current address: Institute of Biology and Nordic Center for Earth Evolution (NordCEE), University of Southern Denmark, Odense, Denmark.

Critical Depth Hypothesis, predicts that phytoplankton blooms begin when the mixed layer shoals to the depth where net phytoplankton growth exceeds net losses (Sverdrup, 1953). In contrast, the *Dilution-Recoupling Hypothesis* predicts initiation of blooms in mid-winter, placing relatively more weight on dilution of grazing pressure because of deep mixing (DM) rather than the enhancement of phytoplankton growth rates from nutrient delivery (Behrenfeld, 2010).

The Bermuda Atlantic Time-Series Study (BATS), initiated in 1988, is one of the lengthiest oceano-graphic time-series studies, and includes complete records of biogeochemical and biological properties of the water column, such as nutrients, cell counts and phytoplankton pigments (Steinberg *et al.*, 2001; Lomas *et al.*, 2010), as well as extensive physical

482

and meteorological measurements (Michaels and Knap, 1996). Furthermore, several studies have addressed prokaryotic population dynamics at BATS (Morris *et al.*, 2005; Carlson *et al.*, 2009; Treusch *et al.*, 2009). Annual convective mixing at BATS results in the entrainment of nutrients into the photic zone initiating an annual spring phytoplankton bloom that results in carbon export (Steinberg *et al.*, 2001). These and other systemic biological responses to nutrient variations are well described (see Michaels and Knap, 1996; Steinberg *et al.*, 2001 and citations within). Patterns of primary production (Menzel and Ryther, 1960; Lohrenz *et al.*, 1992; Michaels and Knap, 1996; Steinberg *et al.*, 2001) and the temporal variability of specific phytoplankton groups have been studied extensively at BATS with a variety of approaches, including radiotracers (Brzezinski and Nelson, 1995; Nelson and Brzezinski, 1997), photosynthetic pigment proxies (Bidigare *et al.*, 1990; Goericke, 1998; Steinberg *et al.*, 2001; Lomas and Bates, 2004), flow cytometric measurements of phytoplankton abundance (Olson *et al.*, 1990; Li *et al.*, 1992; DuRand *et al.*, 2001) and growth (Li *et al.*, 1992; Worden and Binder, 2003a, b; Cuvelier *et al.*, 2010). Most notably, a recent study at BATS showed a >50% increase in chlorophyll *a* (Chl *a*) data between 1996 and 2007 (Lomas *et al.*, 2010).

In subtropical and tropical open-ocean environments, phytoplankton are typically dominated numerically by marine cyanobacteria, specifically *Prochlorococcus* and *Synechococcus*. However, although lower in abundance, eukaryotic taxa can be important in these systems. For example, photosynthetic picoeukaryotes, eukaryotic phytoplankton that are <2–3 µm in size, have been shown to be responsible for 68% of the primary production in the North Atlantic (Li *et al.*, 1993). Their large contribution to production is due to both their size, which is greater than their cyanobacterial counterparts and their high growth rates (Worden *et al.*, 2004). Thus, although photosynthetic picoeukaryotes contributed a maximum of 10% to the ultraphytoplankton (*Synechococcus*, *Prochlorococcus* and eukaryotic phytoplankton <3 µm) cell counts in a North Atlantic study (Li, 1995), they contributed significantly more to primary production (Li, 1994). In Sargasso Sea surface waters, uncultured pico-prymnesiophytes have been shown to contribute roughly equally to primary production as *Prochlorococcus* at the surface (Cuvelier *et al.*, 2010). This group of uncultured eukaryotic phytoplankton is responsible for 25% of total phytoplankton primary production in other North Atlantic regions (Jardillier *et al.*, 2010). Another geographically widespread group of pico-phytoplankton belongs to the order Mamiellales within the prasinophytes. Although pigment-based methods have addressed prasinophyte dynamics as a whole, it has become clear that specific taxa within the Mamiellales have considerable differences in spatial distributions (Foulon *et al.*, 2008; Demir-Hilton *et al.*, 2011). Moreover, it appears that these

taxa are sensitive to environmental change and one, *Micromonas*, has increased numerically in the arctic, where larger phytoplankton taxa have decreased (Li *et al.*, 2009). To date, few studies have quantified contributions of these pico-prasinophytes in the open-ocean, hence there is no baseline established against which future changes can be assessed.

Rappé *et al.*, (1995) identified 16S ribosomal RNA (rRNA) genes derived from eukaryotic plastids in environmental clone libraries and found considerable diversity. Subsequently, a number of other studies have shown extensive diversity within marine eukaryotic phytoplankton communities using 16S rRNA gene clone libraries (Rappé *et al.*, 1997; Brown and Bowman, 2001; Wilmotte *et al.*, 2002; Fuller *et al.*, 2006; Jardillier *et al.*, 2010). These results indicate that there are also many as-of-yet uncultured phytoplankton taxa, similar to findings from environmental 18S rDNA clone libraries (Moon-van der Staay *et al.*, 2001; Not *et al.*, 2007; Viprey *et al.*, 2008; Shi *et al.*, 2009; Cuvelier *et al.*, 2010). Although the diversity of eukaryotic phytoplankton is now appreciated, there is a paucity of data resolving the temporal and spatial distributions of these organisms in open-ocean plankton communities.

In this study, we investigate phytoplankton population dynamics at BATS with a large terminal restriction fragment length polymorphism (T-RFLP) data set previously used to study bacterial plankton community structure (Carlson *et al.*, 2009; Treusch *et al.*, 2009). Plastid 16S rDNA clones were sequenced to identify phytoplankton T-RFLP patterns and quantitative PCR (qPCR) measurements were used to confirm observations of prasinophyte blooms. The data illustrate complex seasonal patterns in phytoplankton turnover that appear to be driven by seasonally changing environmental conditions, and show that an amalgam of spring bloom models is needed to describe the net behavior of phytoplankton in the northwestern Sargasso Sea.

Materials and methods

Sample collection, nucleic acid extraction, community profiling and clone libraries, de-noising, alignment, triplet determination and species identification
Samples and methods described previously are unchanged (Supplementary Table S1, Treusch *et al.*, 2009) and are detailed in brief in supplementary materials. In addition to previously sequenced clones, seven new clones predicted to be of plastid origin based on the observed triplets were sequenced and deposited under the accession numbers JF968594 to JF968600. All newly identified plastid clones were from a clone library constructed from a sample collected in March 2000 at 160 m (BATS138–160).

Enumeration of Mamiellales taxa by qPCR
Samples from a selection of 2003 BATS cruises were analyzed using qPCR. Three qPCR primer-probe sets

were used for detection of Mamiellales, specifically *Bathycoccus*, *Micromonas* and *Ostreococcus*, as described in Demir-Hilton *et al.* (2011). Briefly, field samples were tested for inhibition and triplicate reactions were performed in 25 μl using 1 μl of 1 ng template, 12.5 μl of Taqman Universal Master Mix (Applied Biosystems Foster City, CA, USA) with 2.5 μl of forward and reverse primers (900 nM final concentration) as well as 2.5 μl of probe (250 nM final concentration). Thermal cycling conditions for qPCR were 10 min at 95 °C (initial denaturation), followed by 45 cycles of 15 s at 95 °C and 1 min at 60 °C using an ABI7500 (Applied Biosystems). Data were collected during the annealing phase. Each run included triplicated no-template controls and 10-fold serial dilutions of plasmids containing the targeted 18S rDNA genes, composing the standard curves for each of the respective primer-probe sets. To calculate copy numbers per reaction, linear regression of Ct values against log scale copy numbers of standards were used where threshold and baseline values were calculated for each reaction using the ABI7500 software (Foster City, CA, USA). 18S rDNA copy numbers per reaction were then converted to 18S rDNA copies ml^{-1} based on the use of 1 ng template per reaction, which composed a known fraction of the total DNA extracted from the known volume of seawater filtered at each sampling. Extraction efficiency was assumed to be 100%. One to two copies of the rRNA operon are found in each of the three publicly available *Ostreococcus* genome sequences. Thus, the *Ostreococcus* 18S rDNA copies ml^{-1} values calculated here likely are either equivalent to cells ml^{-1} or twice the number of cells ml^{-1}. For *Bathycoccus*, two copies of the rRNA operon are present in the nuclear genome (Derelle and Moreau, personal communication) and for *Micromonas* 2 (CCMP1545) to 3 (RCC299) are present although genome assembly issues are an issue in this region for *Micromonas* CCMP1545, which may have three copies. The operon copy numbers can again be used to estimate cells ml^{-1} for these taxa.

Environmental data
Pigment and primary production data were downloaded from the BATS webpage (http://bats.bios. edu/), adjusted similarly to the T-RFLP data to the month of DM, and plotted as a composite year (for details, see Carlson *et al.*, 2009; Treusch *et al.*, 2009).

Pearson correlations were determined for environmental measurements, unadjusted to the month of DM, over the duration of the data set. Average plastid signals were obtained by integrating over the entire depth profile (surface to 300 m). Summed nitrate plus nitrite and dissolved phosphate were integrated to the mixed layer depth. Daylight was calculated as the average over each month at the latitude of the BATS site, 32°N.

Results

Overview of the spring bloom in the northwestern Sargasso Sea
Interannual variability in the magnitude and timing of the spring phytoplankton bloom at BATS is determined largely by the timing of maximal convective mixing. Two previous studies, based on the same suite of BATS phytoplankton data from 1990 to 1997 (Steinberg *et al.*, 2001) and additional data extending to 2007 (Lomas *et al.*, 2010) have shown that the bloom can begin as early as January and as late as April. These studies show that the calendar month is irrelevant to the timing of the bloom and that rather the month of DM serves as the best indicator of the bloom onset. Therefore, we aligned data from all years according to their respective month of DM to display inter-relatable annual patterns (Figures 1, 3–6 and Supplementary Table S2) (Carlson *et al.*, 2009; Treusch *et al.*, 2009).

Chl *a* concentrations follow predictable annual patterns during the northwestern Sargasso Sea spring bloom (Figure 1a) (Steinberg *et al.*, 2001; Lomas *et al.*, 2010). Over the period of this data set, Chl *a* standing stock, integrated over the photic zone (0–140 m), increased with the onset of mixing and peaks 2 months following the DM events. Surface chlorophyll concentrations then declined and the deep chlorophyll maximum (DCM) developed between 80 and 120 m during the period of summer stratification. In the upper 5 m, maximum primary production and Chl *a* concentrations coincided with the month of DM (Supplementary Figure S1).

The summed signal from plastid genes contributed up to 10% to the total integrated 16S rRNA gene T-RFLP signal during the spring bloom (Figure 1b). In contrast to Chl *a* concentrations, which peaked in spring 2 months after DM events, the peak integrated T-RFLP plastid signal coincided with DM events (Figure 1b). Thereafter, the T-RFLP plastid signal decreased and was strongest at the DCM. The apparent difference between patterns of plastid abundance and Chl *a* can be attributed to a variety of factors, particularly variation in plastid gene copy number and cell chlorophyll content. Patterns in cyanobacterial distributions (*Prochlorococcus* and *Synechococcus* combined) were essentially the converse of those observed for eukaryotic plastids; cyanobacteria increased as stratification developed and reached a maximum during the period of greatest stratification (Figure 1c). These trends in phytoplankton distributions are similar to those reported in DuRand *et al.* (2001), based on Chl *a* and flow cytometry measurements. The total bacterial count demonstrated some seasonality (Carlson *et al.*, 1996; Steinberg *et al.*, 2001), but was constrained within a range of *ca* 1×10^8–6×10^8 cells l^{-1} throughout the year (Figure 1d).

Integrated plastid abundance (0–300 m) was highly correlated with mixed layer depth, and integrated nitrate and nitrite, but not with integrated
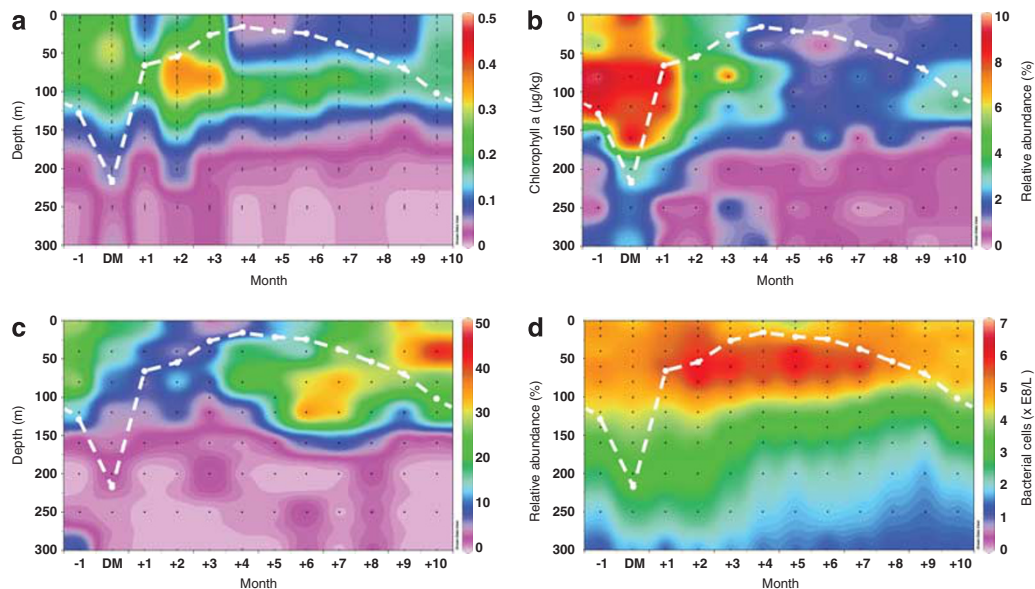
Figure 1 Annual composite of average spatio-temporal distributions of: (**a**) Chl *a*; (**b**) the sum of all identified plastid T-RFLP fragments, plotted as a fraction of the summed T-RFLP signal from all amplified 16S rRNA molecules; (**c**) cyanobacteria (*Synechococcus* and *Prochlorococcus*, reproduced from Treusch *et al.*, 2009); (**d**) 4,6-diamidino-2-phenylindole (DAPI) cell counts. Chlorophyll and DAPI cell counts were taken from the BATS website (http://bats.bios.edu). The white dashed lines indicate the average mixed layer depth that was based on a variable sigma-*t* (potential density) criterion (Sprintall and Tomczak, 1992). MLD was determined as the depth where sigma-*t* is equal to sea surface sigma-*t* plus an increment in sigma-*t* equivalent to a 0.2 °C temperature decrease. Monthly data collected over 10 years was adjusted according to the month of DM and collapsed into a representative composite year (Carlson *et al.*, 2009; Treusch *et al.*, 2009).

Table 1 Pearson correlations of integrated plastid values and environmental variables

	Plastid	Daylight	MLD	N	P
Plastid					
Daylight	0.053				
MLD	**0.617**	−0.675			
N	**0.809**	−0.447	**0.949**		
P	0.346	−0.454	0.434	0.456	

Abbreviations: MLD, mixed layer depth; N, nitrate plus nitrite; P, phosphate.
Bold numbers are significant at $P < 0.05$.

dissolved phosphate or with daylight (Table 1). Dissolved phosphate concentrations are low and frequently undetectable at BATS, making other measures, such as mixed layer depth, a better measure of the delivery of nutrients to mixed layer phytoplankton populations.

Identification of plastid peaks in T-RFLP data
Group-level identification of plastid T-RFLP fragments was based on studies of plastid 16S rRNA genes cloned and sequenced from the BATS site. Phylogenetic reconstruction identified these clones as being derived from the *Prymnesiophyceae*, *Cryptophyceae*, *Prasinophyceae*, *Pelagophyceae*, *Chrysophyceae* and *Bacillariophyceae*, with the latter three groups belonging to the heterokonts (stramenopiles). The phylogenetic distribution of these clones was similar to that seen in an 18S rRNA

gene clone library study conducted at BATS (Not *et al.*, 2007).

Among heterokont clones, BATS138-160-34 was closely related (99.1% identity) to the diatom *Thalassiosira pseudonana*, and another clone (BATS138-160-16) was most closely related to *Rhizosolenia* sp., while a third (SAR04M78) was only distantly related to its nearest neighbors in the *Bacillariophyceae* (Figure 2a). Data shown in Figures 3d, 5e and 6f are a composite of the triplet signals from *Thalassiosira pseudonana* and *Rhizosolenia* sp. These taxa were detected on multiple occasions (Supplementary Figure S3). It is possible their abundance was underestimated because of unusually high genetic variability in the *Bacillariophyceae* at the sites cleaved by the restriction enzymes we used.

BATS138-160-6 and SAR04M64 shared nearly the same T-RFLP triplet but were phylogenetically placed in the *Pelagophyceae* and the *Chrysophyceae*, respectively (Figure 2a), leading us to report a combined signal for pelagophytes and chrysophytes. Dinoflagellates have plastids that appear to have originated from cryptophytes (Keeling, 2010) and could not be resolved from cryptophytes by T-RFLP analysis; therefore, the signal from these two groups was also combined (Figures 3b, 5c and 6d).

Sequences from two genera in the Mamiellales were recovered in the 16S rRNA gene clones. These two *Micromonas* sequences (BATS138-160-20 and SAR04M54) and an *Ostreococcus* sequence (BATS138-160-35) corroborated *in silico* predictions
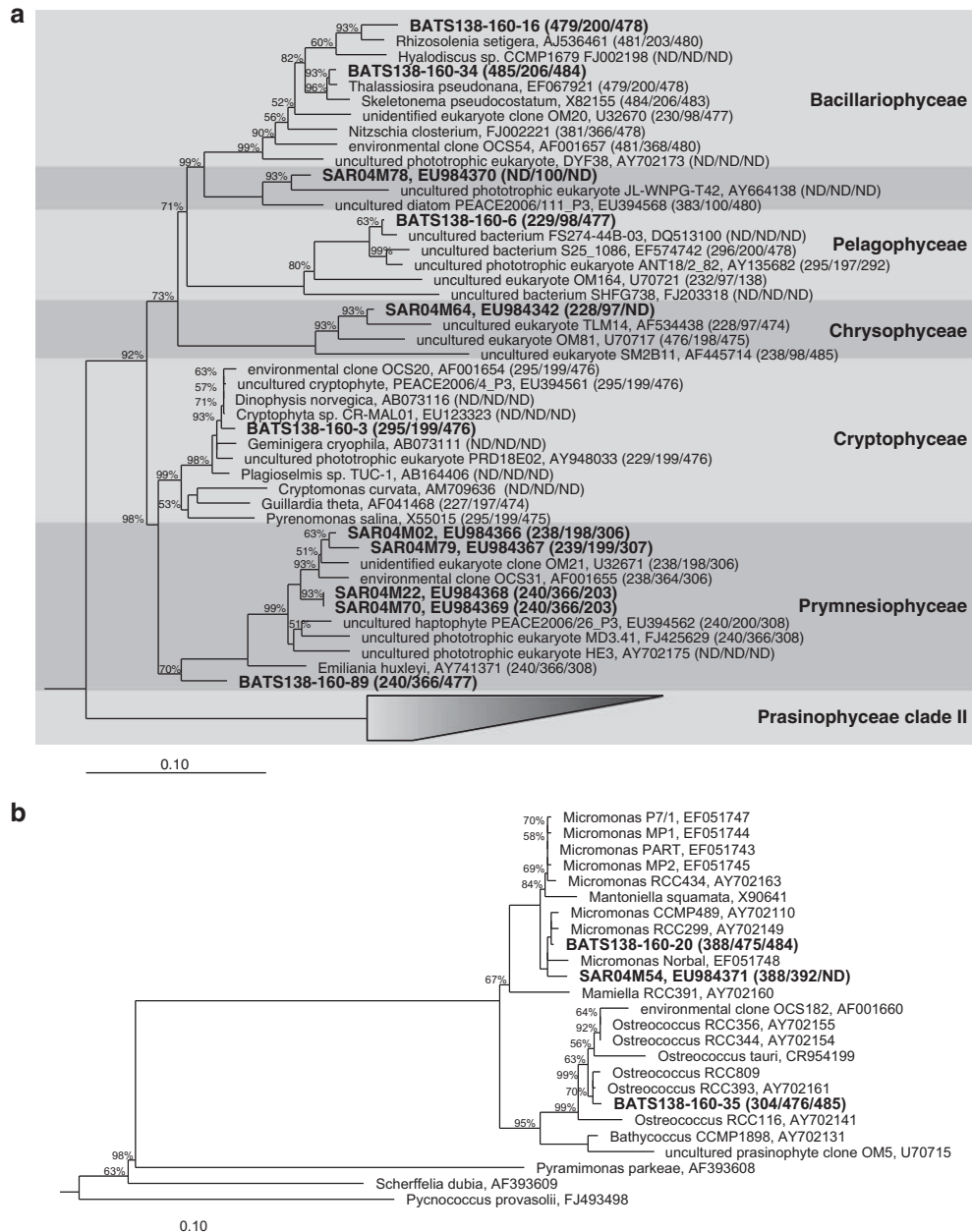
Figure 2 (a) Neighbor-joining distance phylogenetic reconstruction of plastid 16S rRNA genes derived from eukaryotes based on 499 informative positions. Several different lineages were detected, specifically prymnesiophytes (SAR04M02, SAR04M22, SAR04M70 and SAR04M79), diatoms (BATS138-160-16 and BATS138-160-34), pelagophytes (BATS138-160-6), chrysophytes (SAR04M64) and cryptophytes (BATS138-160-3). Bootstrap values over 50% of 1000 replicates are shown. Predicted fragment sizes are indicated in brackets (*Bsu*RI/*Bsh*1236I/*Msp*I). (**b**) Phylogenetic reconstruction of plastid 16S rRNA genes recovered at BATS belonging to pico-prasinophytes within the order Mamiellales. The neighbor-joining distance tree was calculated from 787 informative positions. *Prochlorococcus marinus* str. MIT9313 served as the outgroup. Bootstrap values over 50% of 1000 replicates are indicated. Sequences from a 40 m sample collected in March 2004 (Carlson *et al.*, 2009) were also included and are labeled SAR04M plus clone number in the phylogenetic trees.

(Figure 2b, Supplementary Figure S2). Throughout the manuscript, we use the term 'pico-prasinophyte' to refer to the T-RFLP signal from *Micromonas*, *Ostreococcus* and likely *Bathycoccus*, which we did not recover in the clone libraries, but has been reported previously at Hydrostation S (Anderson *et al.*, 1996) and was resolved using qPCR (see below).

During the assignment of T-RFLP triplets to plastid lineages it became obvious that triplets determined for plastid 16S rRNA gene clones do not necessarily represent the potential diversity within a broad phytoplankton group. *In silico* predictions of triplets for sequences from the SILVA database (Pruesse *et al.*, 2007) confirmed this trend. The Mamiellales were an exception, showing relatively
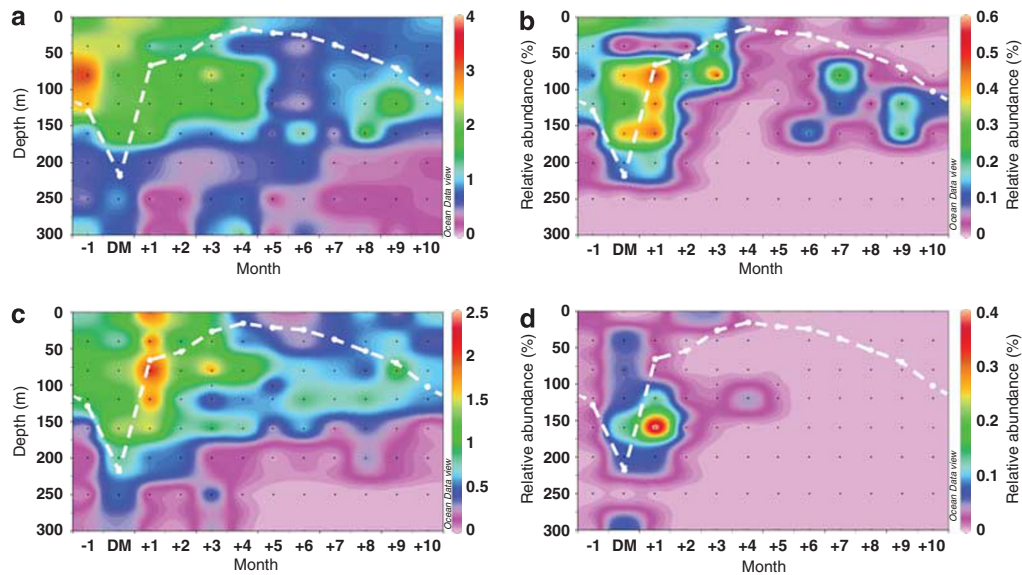
Figure 3 Annual composite of average spatio-temporal distributions of phytoplankton taxa from 12 years of data, adjusted to the month of the maximum mixed layer depth (DM). Shown is the percent abundance of 16S rRNA genes for each group, relative to the total T-RFLP signal: (**a**) prymnesiophytes/OM21; (**b**) dinophytes/cryptophytes; (**c**) pelagophytes/chrysophytes; (**d**) diatoms. Note differences in *z* axis scales.

higher conservation in T-RFLP predictions across the order. Therefore, apart from the pico-prasinophytes, our phylogenetic assignments based on the patterns detected in clones from the BATS site may under-represent overall contributions from some phytoplankton lineages and instead provide insights to particular taxa within these broad groups. This depends on the diversity within each lineage and the extent to which the T-RFLP pattern represented all members. We took a robust approach to data interpretation by relying on T-RFLP patterns from restricted cloned plastid genes for peak identification and also considering the data in the context of all available plastid 16S rRNA gene sequences. The electrophoretic mobility of clones was directly compared with T-RFLP peaks in environmental samples, reducing errors that might result from differences between observed and predicted fragment mobility.

Succession in eukaryotic phytoplankton after DM
Prymnesiophyte blooms developed strongly early in the winter period as the mixed layer began to deepen reaching as high as 1.8–4.8% of the 16S rRNA signal in the surface 80 m 1 month before the timing of maximal convective mixing (Figures 3a, 5b and 6c). The relative contribution of prymnesiophytes remained elevated (0.6–3.8% of the 16S rRNA signal) as the water column stratified, and persisted throughout the euphotic zone for several months post DM.

The relative abundance of dinophytes/cryptophytes increased during the vernal period, however, they remained a minor contributor to the overall phytoplankton population (<0.5%; Figures 3b, 5c

and 6d) during the period of mixing, and were only occasionally detected during the summer (Figures 3b, 5c and 6d). Similarly, pelagophyte/chrysophytes bloomed in the first month after DM although contributing more substantially to the total 16S rRNA signal, ranging from 0.4% to 2.7% (Figures 3c, 5d and 6e). The averaged pelagophyte/chrysophyte signal also extended deeper into the water column, ranging from 0.9% to 2.7% of the 16S rRNA signal at 160 m during month + 1. In the upper 100 m of the water column, their relative contribution remained approximately 1% until the onset of stratification, and persisted at 0.5–1% between 80 and 120 m throughout the summer.

Thalassiosira pseudonana and *Rhizosolenia sp.* like taxa were detected on multiple occasions, but not every year (Supplementary Figure S3). Their average contribution peaked following DM events (Figures 3d, 5e and 6f). Other time-series studies (Steinberg *et al.*, 2001; Lomas *et al.*, 2010) have concluded that diatoms appear episodically at BATS and may be becoming increasingly rare at this site. The period most heavily represented in our data set—1998–2003—corresponds to a period in which diatom abundances were shown to decline at BATS (Lomas *et al.*, 2010). In addition, previous results have shown that when diatoms bloom in the northwestern Sargasso Sea the bloom is ephemeral lasting only days (Krause *et al.*, 2009; Lomas *et al.*, 2009).

Prasinophytes (Figures 4a, 5a and 6b) contributed maximally during the month of DM, on average contributing >5% to the 16S rRNA signal during this period of water column physical instability. Spring bloom pico-prasinophyte populations varied considerably over the years of the study, from below
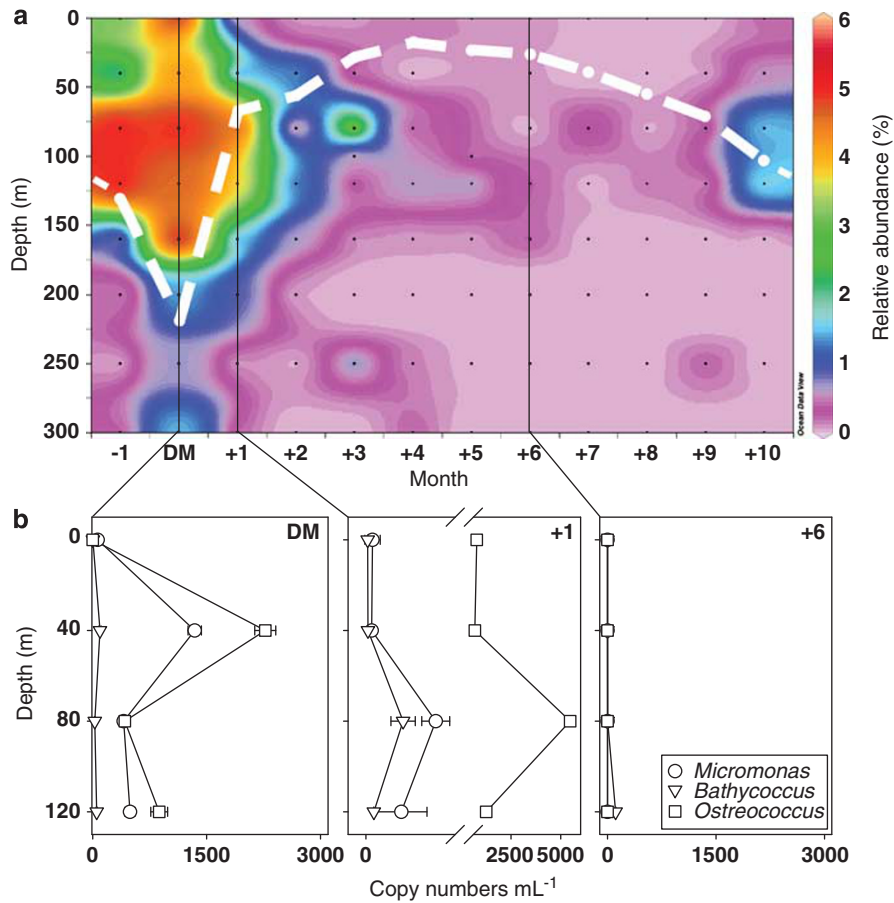
Figure 4 Spatio-temporal distributions of prasinophytes at BATS. (**a**) Average spatio-temporal distributions of prasinophyte 16S rRNA genes, relative to the total T-RFLP signal. (**b**) 18S rDNA copies ml^{-1} enumerated by qPCR for the pico-prasinophytes *Micromonas*, *Ostreococcus* and *Bathycoccus* in depth profiles from the final complete year analyzed using T-RFLP methods (2003). Note differences in *y* axis scales between top and bottom panels.
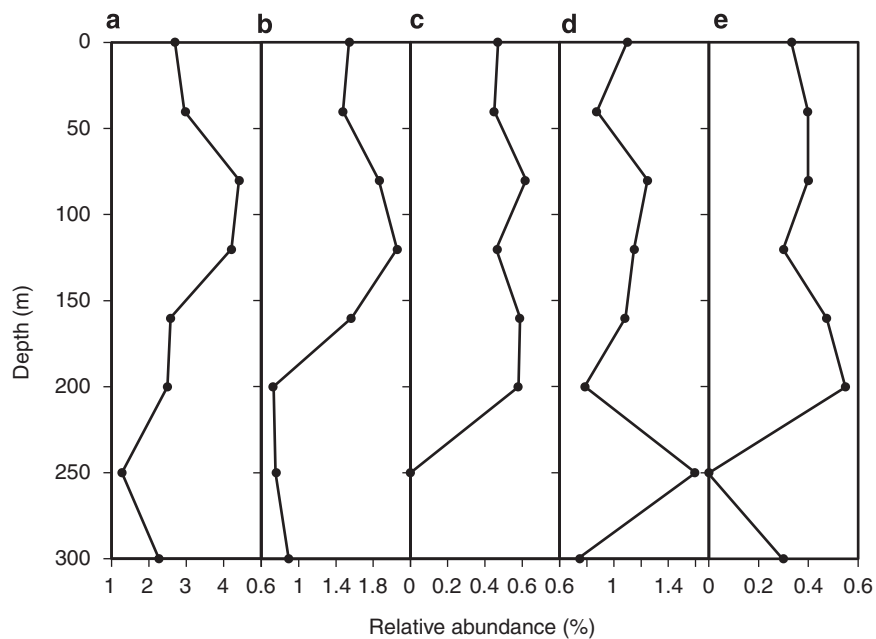

Figure 5 Average distribution of phytoplankton taxa with depth, calculated from the T-RFLP data shown in Figures 3 and 4: (**a**) prasinophytes (see Figure 2a); (**b**) prymnesiophytes/OM21 clade; (**c**) dinophytes/cryptophytes; (**d**) pelagophyte/chrysophyte clades; (**e**) combined signal of diatom clones BATS138-160-16 and BATS138-160-34.
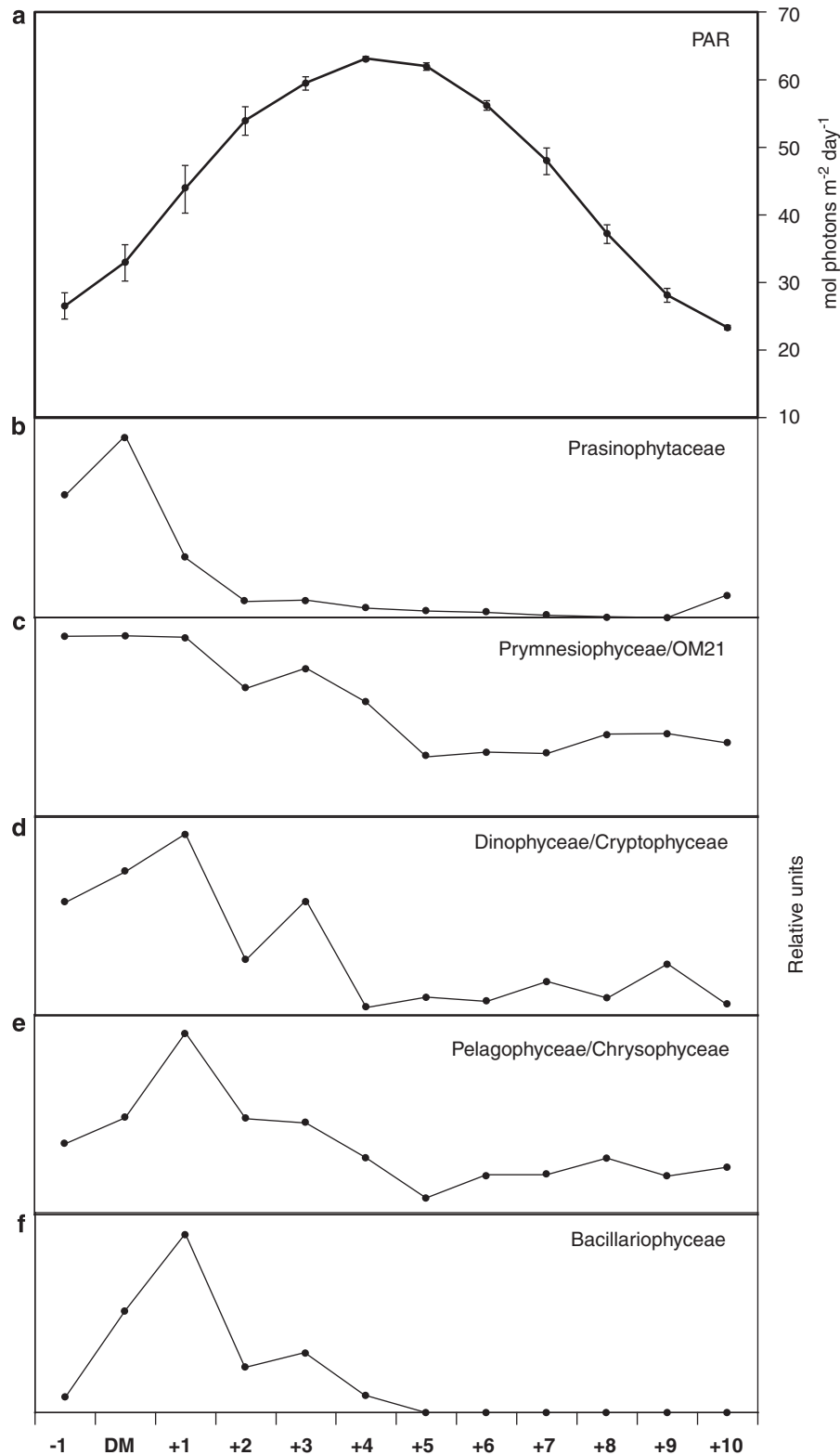
Figure 6 Average seasonal change in relative abundance of phytoplankton taxa, integrated over depth (0–160 m): (**a**) modeled clear sky PAR; (**b**) prasinophytes; (**c**) prymnesiophytes/OM21 clade; (**d**) dinophytes/cryptophytes; (**e**) pelagophytes/chrysophytes and (**f**) bacillariophyte clones BATS138-160-16 and BATS138-160-34 (diatoms). Note that for scaling, the data were normalized to the maximum abundance of the relative fluorescence observed for each taxon.

detection in some years to a maximum of 13.4%. They declined as the surface layer stratified and their signal nearly disappeared once the system was strongly stratified. To evaluate the robustness of the T-RFLP data, we also employed qPCR primer-probe sets to analyze individual genera within the Mamiellales for the final year of the study. qPCR results for *Bathycoccus*, *Micromonas* and *Ostreococcus* showed the same trends as the T-RFLP data for the three cruises investigated (Figure 4). The qPCR results also allowed us to differentiate between the combined T-RFLP pico-prasinophyte signal and revealed that *Ostreococcus* was the numerically dominant Mamiellales in the samples investigated (Figure 4b). Notably, although abundant in samples from relatively shallow depths (40 m, Figure 4b), only clade OII *Ostreococcus* were detected (Figure 2b, BATS138-160-35), which likely represents an open-ocean clade (Demir-Hilton *et al.*, 2011) but was formerly hypothesized to be a deep-adapted clade (Rodriguez *et al.*, 2005).

Patterns in phytoplankton vertical distributions
The lineages detected in our plastid data differed in their vertical distributions (Figure 5). Pico-prasinophytes and prymnesiophytes have similar average maximum abundance peaks, between 80 and 120 m for the former and 120 m for the latter. However, the dinophyte/cryptophyte and pelagophyte/chrysophyte signals were more uniformly distributed throughout the photic zone and extended deeper in the water column. Interestingly, diatoms were not detected in the surface sample (Figure 5e). Plastid T-RFLP signals were also sometimes detected in the mesopelagic, where light should be insufficient for photosynthetic growth, suggesting export from the photic zone (Figures 5a, c–e).

Discussion

16S rRNA gene T-RFLP analysis has previously been shown to deliver reliable, reproducible results for the analysis of large sample sets (reviewed in Nocker *et al.*, 2007). In some cases, it has been shown to be more sensitive than pigment analyses (Stachowski-Haberkorn *et al.*, 2009), although clearly it complements such analyses and is subject to different biases. Of these the most significant is likely to be variation in gene copy number between different phytoplankton species; there are two copies of the 16S rRNA gene in many plastid genomes, but many phytoplankton species contain more than one plastid, and plastids can contain many genome copies (Ersland *et al.*, 1981). For this and other reasons, T-RFLP data provide only a relative indication of cellular abundances. The fact that qPCR analysis of pico-prasinophyte genera at BATS corresponded well with the T-RFLP data provides one example confirming the reliability of T-RFLP for

measurements of relative microbial abundance (Figure 4). Many of the interesting observations that emerged from this T-RFLP analysis are based on the broad taxonomic range and comparative power of this technique, including the early bloom onset and seasonal succession of taxa, and the depth differentials observed between taxa (Figure 6).

Succession in eukaryotic phytoplankton
We observed blooms of the pico-prasinophytes *Ostreococcus* and *Micromonas* that have not previously been reported in the open-ocean (Figures 4a and b). These taxa have reduced genomes and are distributed throughout tropical and temperate regions of the oceans; *Micromonas* and *Bathycoccus* are also found in Arctic systems (Lovejoy *et al.*, 2007; Worden *et al.*, 2009). Little quantitative data exists for this suite of taxa in open-ocean settings. The blooms observed here occurred during and just after the deep winter mixing period (months 0 (DM) and +1) with a decline in contributions through the remainder of the year. Thus the distribution of *Ostreococcus* and *Micromonas* appears to be related to factors associated with DM rather than day length. This supports the hypothesis that the primary determinant of interannual variability in these populations is nutrient input caused by deep convective mixing. Our data are consistent with the observations of Lomas and Bates (2004) who attributed 2–8% of integrated Chl *a* stocks at BATS to prasinophytes during spring, based on high-performance liquid chromatography measurements of prasinoxanthin. However, in contrast to our T-RFLP and qPCR results, Goericke (1998) found that prasinophytes were not abundant between March 1986 and February 1987 based on high-performance liquid chromatography data. Our qPCR analyses (Figure 4b) indicated there were up to 5478 ± 164 *Ostreococcus* 18S rDNA copies ml^{-1}, likely relating to ~ 2739 or 5478 cells ml^{-1}, depending on whether one or two copies of the operon are present in the genome, respectively. The discrepancy between this study and that of Goericke (1998) is likely due to the fact that in the latter samples were not collected between March and June (with March roughly corresponding to a common time for the DM event). Low prasinophyte contributions at other times of the year reported by Goericke are consistent with our observations, as were other results, such as relatively low overall contributions of dinophytes/cryptophytes and diatoms. Overall, the periods of highest pico-prasinophyte contributions (Figure 4) track periods during which picocyanobacteria as a whole had the lowest contributions to the overall 16S rRNA gene signal (Figure 1c).

Our study revealed that prymnesiophytes consistently form an intense bloom early in the year. In contrast to the pico-prasinophytes, the bloom was before the DM event. Moreover, their contributions remained high throughout spring mixing, into early

490

summer as the water column stratified (that is, $+4$, Figure 3a) and their contributions remained substantial at the DCM for the remainder of the year (Figures 5b and 6c). Given that the clones used to identify the prymnesiophyte T-RFLP signal were broadly distributed across this group, these trends do not preclude a shift from one prymnesiophyte taxon (for example, coccolithophores; which previously have been reported for wintertime in this region) to another (Figure 2a). High-performance liquid chromatography studies indicate that most of the prymnesiophyte biomass is in the picoplankton size fraction (for example, Goericke, 1998). More recently, molecular approaches have shown that pico-prymnesiophytes comprise $\sim 25\%$ of the pico-phytoplankton biomass in the Atlantic, with increasing contributions at higher latitudes (Cuvelier et al., 2010; Jardillier et al., 2010). In the Sargasso Sea, they have been shown to contribute $\sim 22\%$ of picophytoplankton carbon at the surface and DCM (Cuvelier et al., 2010). Both Jardillier et al. (2010) and Cuvelier et al. (2010) also showed that the pico-prymnesiophytes responsible for much of this biomass and production were from uncultured taxa. The 16S rDNA sequences retrieved here also appeared to be from uncultured prymnesiophytes (Figure 2a).

The DCM
The persistence of the chlorophyll signal in the DCM throughout the summer (Figure 1a) reflects both a shift in the distribution of phototrophs to greater depths as surface nutrients become depleted and the influence of photoadaptation, which causes an offset between the DCM and the region of highest phytoplankton density and water column productivity. At BATS, the DCM phytoplankton community is numerically dominated by picocyanobacteria (Figure 1c), specifically *Prochlorococcus* (for example, DuRand et al., 2001). As discussed above the cellular biomass of eukaryotic phytoplankton taxa are greater than that of the picocyanobacteria, hence even when fairly low in abundance their biomass contributions are likely still significant. Like Steinberg et al. (2001), we observed prymnesiophytes in the region of the DCM during periods of intense water column stratification. We also observed pelagophytes in the DCM, but their overall contributions appeared low, about 1% of T-RFLP signal (Figures 3c, 5d and 6e). Steinberg et al. (2001) also observed pelagophytes in the DCM but concluded they were among the most abundant eukaryotic phytoplankton at BATS. Although these data are in contrast to our findings, the dates of their study do not overlap significantly with ours. Hence, it is possible this discrepancy reflects ecosystem level changes, as reported for diatoms (Lomas et al., 2010). The observation of pelagophytes and other taxa in the summer DCM might have implications for understanding the genesis of the spring bloom;

populations that endure the summer in the relative refuge of the DCM could seed blooms as the mixed layer deepens during the winter. But, at present, not enough is known about phytoplankton diversity to be certain that the taxa that occur in the region of the DCM are genetically and phenotypically identical to those that constitute winter and spring bloom populations.

Spring bloom models
Behrenfeld (2010) and Sverdrup (1953) provided a relatively broad theoretical basis for understanding how physical, chemical and biological factors might interact to control phytoplankton bloom dynamics. Others have modified these concepts by considering the impact of variations between ocean regions. For example, Siegel et al. (2002) proposed that there are two distinct regimes for spring bloom dynamics in the North Atlantic Ocean. North of 40°N, the pattern follows Sverdrup's (1953) hypothesis. South of 40°N, where mixing is reduced and depth of the euphotic zone is often >100 m, it was proposed that nutrients, rather than light, are the limiting factor, causing the spring bloom to be initiated early. According to this low(er) latitude model, nutrients entrained into the euphotic zone during convective mixing trigger a phytoplankton bloom in advance of mixed layer shoaling. Thus BATS, located at 32°N, was considered to be outside the region where Sverdrup's hypothesis applies.

Our observations show clearly that mixing drives the timing of the earliest blooms of phytoplankton taxa. This conclusion is supported by correlations (or lack thereof) between integrated stocks of N and P, mixed layer depth, day length, and the integrated plastid signal (Table 1). The low correlation between the integrated plastid signal and dissolved phosphate is unsurprising because phosphate is rapidly reduced to undetectable levels after its delivery into the euphotic zone by mixing events. These data fit predictions of Behrenfeld's *Dilution-Recoupling Hypothesis,* which emphasizes the relaxation of predation caused by the dilution of predators and prey as the mixed layer deepens. But the data are also consistent with Siegel's hypothesis (2002) that the mixing of nutrients into the photic zone initiates the spring bloom in the northwestern Sargasso Sea. The data we present do not distinguish between these possibilities. However, the data do illustrate details of the diversification of phytoplankton into niche space at BATS and contribute to the perspective that phytoplankton turnover is driven by changing physical and biogeochemical conditions over the course of the annual spring bloom in the northwestern Sargasso Sea. As Siegel and coworkers highlight, laboratory measurements have ascribed Ic values ranging from 0.1 to 0.8 mol photons m^{-2} day^{-1}, to different phytoplankton species, which could dramatically alter growth rates during winter mixing when incident photosynthetically active

radiation (PAR) is low (Figure 6a) and cells spend more time deeper in the water column as a result of advection (Siegel et al., 2002). Other factors, such as adaptations for predator or virus evasion, half saturation constants for nutrients, and differing temperature optima, might also have important roles in determining the temporal distribution of phytoplankton blooms. For example, pico-prymnesiophyte adaptations to low nutrients inferred from population level genome sequence data, are consistent with their presence during stratified conditions observed here (Cuvelier et al., 2010). Our results provide insight into the partitioning of the niche space by phytoplankton taxa at BATS. These insights should facilitate development and testing of mechanistic hypotheses about factors controlling these taxa, and may lead to improved predictions of phytoplankton responses to changes in ocean conditions.

Acknowledgements

References

Anderson R, Bidigare R, Keller M, Latasa M. (1996). A comparison of HPLC pigment signatures and electron microscopic observations for oligotrophic waters of the North Atlantic and Pacific Oceans. *Deep-Sea Res II* **43**: 517–537.

Behrenfeld MJ. (2010). Abandoning Sverdrup's critical depth hypothesis on phytoplankton blooms. *Ecol* **91**: 977–989.

Bidigare RR, Marra J, Dickey TD, Iturriaga R, Baker KS, Smith RC et al. (1990). Evidence for phytoplankton succession and chromatic adaptation in the Sargasso Sea during Spring 1985. *Marine Ecol Prog Ser* **60**: 113–122.

Brown MV, Bowman JP. (2001). A molecular phylogenetic survey of sea-ice microbial communities (SIMCO). *FEMS Microbiol Ecol* **35**: 267–275.

Brzezinski MA, Nelson DM. (1995). The annual silica cycle in the Sargasso Sea near Bermuda. *Deep-Sea Res I-Oceanograph Res Papers* **42**: 1215–1237.

Carlson CA, Ducklow HW, Sleeter TD. (1996). Stocks and dynamics of bacterioplankton in the northwestern Sargasso Sea. *Deep Sea Res II-Topical Stud Oceanograph* **43**: 491–516.

Carlson CA, Morris RM, Parsons R, Treusch AH, Giovannoni SJ, Vergin K. (2009). Seasonal dynamics of SAR11 populations in the euphotic and mesopelagic zones of the northwestern Sargasso Sea. *ISME J* **3**: 283–295.

Cuvelier ML, Allen AE, Monier A, McCrow JP, Messie M, Tringe SG et al. (2010). Targeted metagenomics and ecology of globally important uncultured eukaryotic phytoplankton. *Proc Natl Acad Sci USA* **107**: 14679–14684.

Demir-Hilton E, Sudek S, Cuvelier ML, Gentemann CL, Zehr JP, Worden AZ. (2011). Global distribution patterns of distinct clades of the photosynthetic picoeukaryote *Ostreococcus*. *ISME J* **5**: 1095–1107.

DuRand MD, Olson RJ, Chisholm SW. (2001). Phytoplankton population dynamics at the Bermuda Atlantic Time-series station in the Sargasso Sea. *Deep-Sea Res II-Topical Stud Oceanograph* **48**: 1983–2003.

Ersland DR, Aldrich J, Cattolico RA. (1981). Kinetic complexity, homogeneity, and copy number of chloroplast DNA from the marine alga *Olisthodiscus luteus*. *Plant Phys* **68**: 1468–1473.

Foulon E, Not F, Jalabert F, Cariou T, Massana R, Simon N. (2008). Ecological niche partitioning in the picoplanktonic green alga *Micromonas pusilla*: evidence from environmental surveys using phylogenetic probes. *Environ Microbiol* **10**: 2433–2443.

Fuller NJ, Campbell C, Allen DJ, Pitt FD, Zwirglmaierl K, Le Gall F et al. (2006). Analysis of photosynthetic picoeukaryote diversity at open ocean sites in the Arabian Sea using a PCR biased towards marine algal plastids. *Aquatic Microb Ecol* **43**: 79–93.

Goericke R. (1998). Response of phytoplankton community structure and taxon-specific growth rates to seasonally varying physical forcing in the Sargasso Sea off Bermuda. *Limnol Oceanog* **43**: 921–935.

Jardillier L, Zubkov MV, Pearman J, Scanlan DJ. (2010). Significant CO2 fixation by small prymnesiophytes in the subtropical and tropical northeast Atlantic Ocean. *ISME J* **4**: 1180–1192.

Keeling PJ. (2010). The endosymbiotic origin, diversification and fate of plastids. *Philosophical Trans R S B-Biol Sci* **365**: 729–748.

Krause JW, Nelson DM, Lomas MW. (2009). Biogeochemical responses to late-winter storms in the Sargasso Sea. II. Increased rates of biogenic silica production and export. *Deep-Sea Res I* **56**: 861–874.

Li WK, Dickie PM, Irwin BD, Wood AM. (1992). Biomass of bacteria, cyanobacteria, prochlorophytes and photosynthetic eukaryotes in the Sargasso Sea. *Deep Sea Res* **39**: 501–519.

Li WKW. (1994). Primary production of Prochlorophytes, Cyanobacteria, and Eukaryotic ultraphytoplankton—measurements from flow cytometric sorting. *Limnol Oceanog* **39**: 169–175.

Li WKW. (1995). Composition of ultraphytoplankton in the central North-Atlantic. *Mar Ecol Prog Ser* **122**: 1–8.

Li WKW, Dickie PM, Harrison WG, Irwin BD. (1993). Biomass and production of bacteria and phytoplankton during the spring bloom in the western North-Atlantic Ocean. *Deep-Sea Res II-Topical Stud Oceanograph* **40**: 307–327.

Li WKW, McLaughlin FA, Lovejoy C, Carmack EC. (2009). Smallest algae thrive as the Arctic Ocean freshens. *Science* **326**: 539.

Lohrenz SE, Knauer GA, Asper VL, Tuel M, Michaels AF, Knap AH. (1992). Seasonal variability in primary production and particle-flux in the northwestern Sargasso Sea—United-States JGOFS Bermuda Atlantic Time-Series Study. *Deep-Sea Res Part I -Oceanograph Res Papers* **39**: 1373–1391.

Lomas MW, Bates NR. (2004). Potential controls on interannual partitioning of organic carbon during the winter/spring phytoplankton bloom at the Bermuda Atlantic Time-series Study (BATS) site. *Deep-Sea Res - Oceanograph Res Papers* **51**: 1619–1636.

Lomas MW, Lipschultz F, Nelson DM, Krause JW, Bates NR. (2009). Biogeochemical responses to late-winter storms in the Sargasso Sea. I. Pulses of primary and new production. *Deep-Sea Res I* **56**: 843–860.

Lomas MW, Steinberg DK, Dickey T, Carlson CA, Nelson NB, Condon RH *et al.* (2010). Increased ocean carbon export in the Sargasso Sea linked to climate variability is countered by its enhanced mesopelagic attenuation. *Biogeosciences* **7**: 57–70.

Lovejoy C, Vincent WF, Bonilla S, Roy S, Martineau MJ, Terrado R *et al.* (2007). Distribution, phylogeny, and growth of cold-adapted picoprasinophytes in arctic seas. *J Phycol* **43**: 78–89.

Menzel DW, Ryther JH. (1960). The annual cycle of primary production in the Sargasso Sea off Bermuda. *Deep-Sea Res* **6**: 351–367.

Michaels AF, Knap AH. (1996). Overview of the US JGOFS Bermuda Atlantic Time-series Study and the Hydro-station S program. *Deep-Sea Res II-Topical Stud Oceanograph* **43**: 157–198.

Moon-van der Staay SY, De Wachter R, Vaulot D. (2001). Oceanic 18S rDNA sequences from picoplankton reveal unsuspected eukaryotic diversity. *Nature* **409**: 607–610.

Morris RM, Vergin KL, Cho JC, Rappé MS, Carlson CA, Giovannoni SJ. (2005). Temporal and spatial response of bacterioplankton lineages to annual convective overturn at the Bermuda Atlantic Time-series Study site. *Limnol Oceanog* **50**: 1687–1696.

Nelson DM, Brzezinski MA. (1997). Diatom growth and productivity in an oligotrophic midocean gyre: a 3-yr record from the Sargasso Sea near Bermuda. *Limnol Oceanog* **42**: 473–486.

Nocker A, Burr M, Camper AK. (2007). Genotypic microbial community profiling: a critical technical review. *Microb Ecol* **54**: 276–289.

Not F, Gausling R, Azam F, Heidelberg JF, Worden AZ. (2007). Vertical distribution of picoeukaryotic diversity in the Sargasso Sea. *Environ Microbiol* **9**: 1233–1252.

Olson RJ, Chisholm SW, Zettler ER, Altabet MA, Dusenberry JA. (1990). Spatial and temporal distributions of prochlorophyte picoplankton in the North Atlantic Ocean. *Deep-Sea Res* **37**: 1033–1051.

Pruesse E, Quast C, Knittel K, Fuchs BM, Ludwig WG, Peplies J *et al.* (2007). SILVA: a comprehensive online resource for quality checked and aligned ribosomal RNA sequence data compatible with ARB. *Nucleic Acids Res* **35**: 7188–7196.

Rappé MS, Kemp PF, Giovannoni SJ. (1995). Chromophyte plastid 16S ribosomal RNA genes found in a clone library from Atlantic Ocean seawater. *J Phycol* **31**: 979–988.

Rappé MS, Kemp PF, Giovannoni SJ. (1997). Phylogenetic diversity of marine coastal picoplankton 16S rRNA genes cloned from the continental shelf off Cape Hatteras, North Carolina. *Limnol Oceanog* **42**: 811–826.

Rodriguez F, Derelle E, Guillou L, Le Gall F, Vaulot D, Moreau H. (2005). Ecotype diversity in the marine picoeukaryote Ostreococcus (Chlorophyta, Prasinophyceae). *Environ Microb* **7**: 853–859.

Shi XL, Marie D, Jardillier L, Scanlan DJ, Vaulot D. (2009). Groups without cultured representatives dominate eukaryotic picophytoplankton in the oligotrophic South East Pacific Ocean. *PLoS One* **4**: e7657.

Siegel DA, Doney SC, Yoder JA. (2002). The North Atlantic spring phytoplankton bloom and Sverdrup's critical depth hypothesis. *Science* **296**: 730–733.

Sprintall J, Tomczak M. (1992). Evidence of the barrier layer in the surface layer of the tropics. *J Geophys Res* **97**: 7305–7316.

Stachowski-Haberkorn S, Quiniou L, Beker B, Haberkorn H, Marie D, de la Broise D. (2009). Comparative study of three analysis methods (TTGE, flow cytometry and HPLC) for xenobiotic impact assessment on phytoplankton communities. *Ecotox* **18**: 364–376.

Steinberg DK, Carlson CA, Bates NR, Johnson RH, Michaels AF, Knap AH. (2001). Overview of the US JGOFS Bermuda Atlantic Time-series Study (BATS): a decade-scale look at ocean biology and biochemistry. *Deep-Sea Res II* **48**: 1405–1447.

Sverdrup HU. (1953). On conditions for the vernal blooming of phytoplankton. *J Cons Perm Int Explor Mer* **18**: 287–295.

Treusch AH, Vergin KL, Finlay LA, Donatz MG, Burton RM, Carlson CA *et al.* (2009). Seasonality and vertical structure of microbial communities in an ocean gyre. *ISME J* **3**: 1148–1163.

Viprey M, Guillou L, Ferreol M, Vaulot D. (2008). Wide genetic diversity of picoplanktonic green algae (Chloroplastida) in the Mediterranean Sea uncovered by a phylum-biased PCR approach. *Environ Microbiol* **10**: 1804–1822.

Wilmotte A, Demonceau C, Goffart A, Hecq JH, Demoulin V, Crossley AC. (2002). Molecular and pigment studies of the picophytoplankton in a region of the Southern Ocean (42-54 degrees S, 141-144 degrees E) in March 1998. *Deep-Sea Res II-Topical Stud Oceanograph* **49**: 3351–3363.

Worden AZ, Binder BJ. (2003a). Application of dilution experiments for measuring growth and mortality rates among Prochlorococcus and Synechococcus populations in oligotrophic environments. *Aqua Microbl Ecol* **30**: 159–174.

Worden AZ, Binder BJ. (2003b). Growth regulation of rRNA content in Prochlorococcus and Synechococcus (marine cyanobacteria) measured by whole-cell hybridization of rRNA-targeted peptide nucleic acids. *J Phycol* **39**: 527–534.

Worden AZ, Lee JH, Mock T, Rouze P, Simmons MP, Aerts AL *et al.* (2009). Green evolution and dynamic adaptations revealed by genomes of the marine picoeukaryotes micromonas. *Science* **324**: 268–272.

Worden AZ, Nolan JK, Palenik B. (2004). Assessing the dynamics and ecology of marine picophytoplankton: the importance of the eukaryotic component. *Limnol Oceanog* **49**: 168–179.

Supplementary Information accompanies the paper on The ISME Journal website (http://www.nature.com/ismej)